Bidirectional soft-switching DC/DC converter for highly efficient EV chargers: Comprehensive analysis of a 20 kW CLLLC converter prototype for Vehicle-to-Grid (V2G)

Matthias Luh[1], Thomas Blank[1], Marc Weber[1]

[1] Institute for Data Processing and Electronics (IPE), Karlsruhe Institute of Technology (KIT), Germany

Corresponding author: Matthias Luh, Matthias.Luh@kit.edu

Abstract

The increasing utilization of high-power chargers for electric vehicles (EV) and electricity from renewable energy poses major challenges. Emerging topologies such as the CLLLC converter can be key enablers for powerful yet inexpensive EV charging and may also improve integration of renewables into the grid. The CLLLC converter, a bidirectional, galvanically isolated, soft switching DC/DC converter, can be used to charge EVs or return energy to the grid. This paper presents theory, design and results of a 20 kW CLLLC converter prototype using SiC MOSFETs and synchronous rectifying with an efficiency of 98 %.

1 Introduction

Within the last decade, supply and demand for electric vehicles (EV) has increased tremendously. CO2 emissions in the transport sector and the dependency on fossil fuels can be reduced with EVs due to their potential to charge from renewable energy sources and lower energy consumption compared to internal combustion engine vehicles [1]. The large number of EVs to be charged in the future as well as an increasing share of renewable energies pose major challenges for transmission and distribution grids in many countries. However, given the enormous cumulative storage capacity of future EVs, they could also play an important role in temporarily storing energy of only partially controllable solar and wind power plants and thus present a great chance for grid stability. This technology, known as Vehicle-to-Grid (V2G), is not new [2], but could become economically attractive [3] due to the energy storage demand, increased cycle stability of modern battery cells and their falling market prices. To charge an EV, electrical energy is transported unidirectionally from the grid to the battery. If the EV shall deliver energy back to the grid as well, a bidirectional charger is required.

2 Theory

2.1 Resonant converters in EV chargers

An essential part of EV chargers is the DC/DC converter [4], which converts the DC voltage generated by the grid-connected AC/DC converter into the voltage required by the battery. A significant part of losses that occur in the converters is caused by switching losses in their power semiconductors. Resonant converters can drastically reduce switching losses and thus increase the efficiency and performance of these converters [5]. This is achieved by either reducing the current flowing through (zero-current switching, ZCS) or the voltage across the component (zero-voltage switching, ZVS) to a negligible value at the time of switching. These effects are obtained with the aid of parasitic or supplementary capacitive and inductive components. As a result of the reduced frequency-dependent losses, the switching frequency of the converters can be significantly increased. Wide-bandgap semiconductors (WBG) made of silicon carbide (SiC) and gallium arsenide (GaAs) are particularly suitable for this purpose. When using a higher switching frequency, space, weight and costs can be reduced. This is because the current and voltage swings occurring at the terminals decrease and the input and output filters as well as the high-frequency transformers providing galvanic isolation in DC/DC converters of EV chargers can be dimensioned much smaller [5].

In [5] and [6] resonant switches are discussed, which are essentially semiconductor switches supplemented by an LC resonant circuit. They can replace conventional semiconductor switches in many hard-switching DC-DC converter topologies, resulting in quasi-resonant converters (QRC). However, perhaps the most important topologies

ISBN 978-3-8007-5245-4

for galvanically isolated, resonant DC/DC converters in the kilowatt range are based on the structure depicted in Fig. 1, herein referred to as bridge resonant converters (BRC) [5], [7], [8], [9]. The converter is fed by a DC source – typically a DC voltage – and generates an AC voltage from it in an inverter stage. The resulting AC current passes through the resonant circuit and is rectified on the output side. In many cases, HF transformers or coupled coils are used in the resonant bridge converter, which galvanically isolate input and output similarly to a Dual Active Bridge (DAB). The transformer can also be part of the resonant circuit.

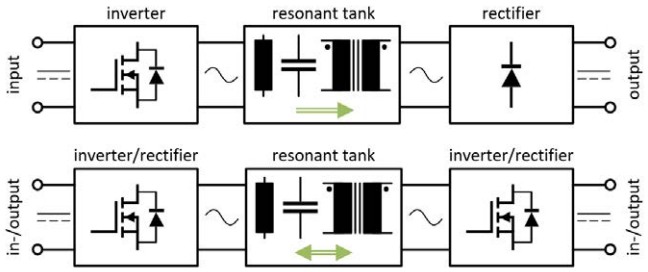

Fig. 1: Fundamental structure of a unidirectional (top) and bidirectional (bottom) BRC

Possible realizations of inverter stages are shown in Fig. 2 while examples of rectifier stages are given in Fig. 3. Stages with three AC-terminals may be used with center-tapped transformers or split capacitor resonant tanks like the LLC converter presented in Fig. 5. There is a large variety of possibilities for the design of the resonant circuit [7], [8], some of which are depicted in Fig. 4.

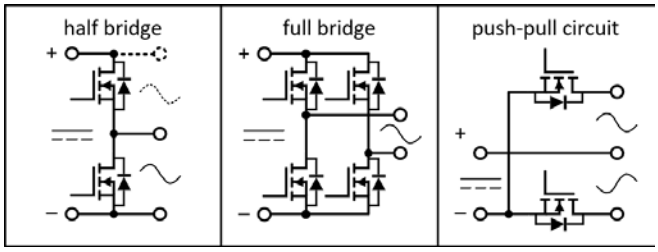

Fig. 2: Examples of inverter stages in BRCs

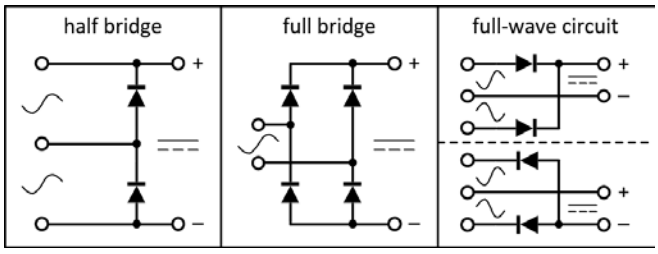

Fig. 3: Examples of rectifier stages in BRCs

In particular, the LLC converter and bidirectional modifications based on it, such as the CLLC or CLLLC converter (upper row of Fig. 4), represent some of the most promising options for galvanically isolated DC/DC converters. They are able to cover a wide range of input to output voltage ratios and achieve high power density and efficiency, thereby representing an ideal choice for high-performance EV battery chargers [10], [11], [12].

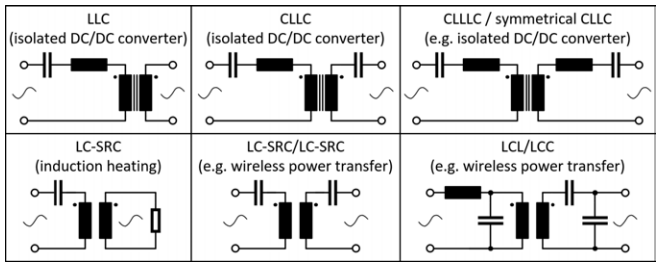

Fig. 4: Selection of resonant tank circuits in BRCs

Although it is possible to operate LLC converters in reverse direction if active rectifiers are used, significantly higher switching losses can occur in this operation. Thus, the advantages of the LLC over the simpler dual active bridge (DAB) are less dominant [13]. In EVs, the use of LLC converters in bidirectional operation is conceivable with low reverse direction power, such as for the operation of AC sockets from the battery for EV passengers. For higher reverse direction powers, like in a bidirectional 20 kW V2G charger, the LLC converter is less suitable. Since the CLLLC converter looked most promising for this application but prototypes presented in literature were rare in this power class, we chose the CLLLC converter topology presented in this paper. The topology is also referred to as CLLC [12], [14] or symmetric CLLC [9] converter by other authors. To avoid confusion with CLLC converters, which consist of only one resonant inductor [9], [15], [16], this paper explicitly refers to the CLLLC converter as in [17] and [18].

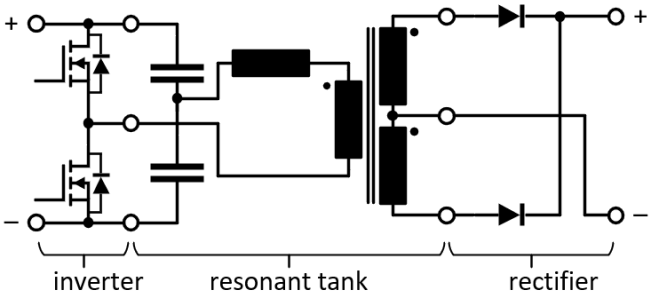

Fig. 5: LLC converter with half bridge inverter and full-wave rectifier, resonant tank with split capacitor and center tapped transformer configuration

2.2 Operation of the CLLLC converter

The CLLLC converter shown in Fig. 6 uses two full bridges comprising MOSFETs, their body diodes and parasitic capacitances C_{DS}. The resonant tank

consists of the transformer T1 as well as serial capacitances C_{R1}/C_{R2} and inductances L_{R1}/L_{R2}. The operating principle with forward power flow of the CLLLC converter is very similar to the one of the LLC converter. In contrast to a bidirectional LLC converter, the basic principle remains the same in the backward operation of a CLLLC converter. The MOSFETs on the input/primary side are driven complementarily in pairs to generate a square wave voltage across the input of the resonant circuit (upper plot). In general, the duty cycle is 50 %. The switching behavior is explained with the measurements of the prototype in Fig. 7:

At t_0, Q1/Q4 are already turned on and Q2/Q3 are off, so the resonant tank voltage V_{res1} is positive. I_{res1} is positive as well and begins to fall.

Q1 and Q4 turn off at t_1. Since I_{res1} is carried by L_{R1}, it remains positive and therefore charges the parasitic capacitances C_{DS} of the formerly conducting FETs Q1/Q4 while discharging the ones of Q2/Q3. As a result, the resonant tank voltage V_{res1} changes gradually while crossing zero volts at t_2 and reaching the opposite voltage at t_3. Extra capacitors parallel to the FETs can reduce dV_{res1}/dt.

After the drain-source capacitances of Q2/Q3 are discharged and V_{DS} becomes negative, their body-diodes conduct the resonant tank current I_{res1} at t_3.

Before I_{res1} changes its sign at t_5, the MOSFETs Q2 and Q3 turn on at t_4. As their V_{DS} was already approximately 0 V, they turn on with zero voltage switching (ZVS), hence eliminating switching losses. If a fast turn-off of Q1/Q4 is achieved at t_1, switching losses are negligible at turn-off as well. This process is repeated vice versa.

On the output/secondary side, the MOSFET capacitances are also (dis-)charged by the resonant tank current: After I_{res2} changes its sign at t_6, the resonant tank voltage is reversed until t_7 for this reason. The body-diodes stop conducting the resonant tank current as it reaches 0 A at t_6, therefore switching losses are eliminated by zero current switching (ZCS) on the output side. Antiparallel freewheeling diodes or synchronous rectifying utilizing MOSFETs Q5-Q8 can be used to significantly reduce conducting losses at the output.

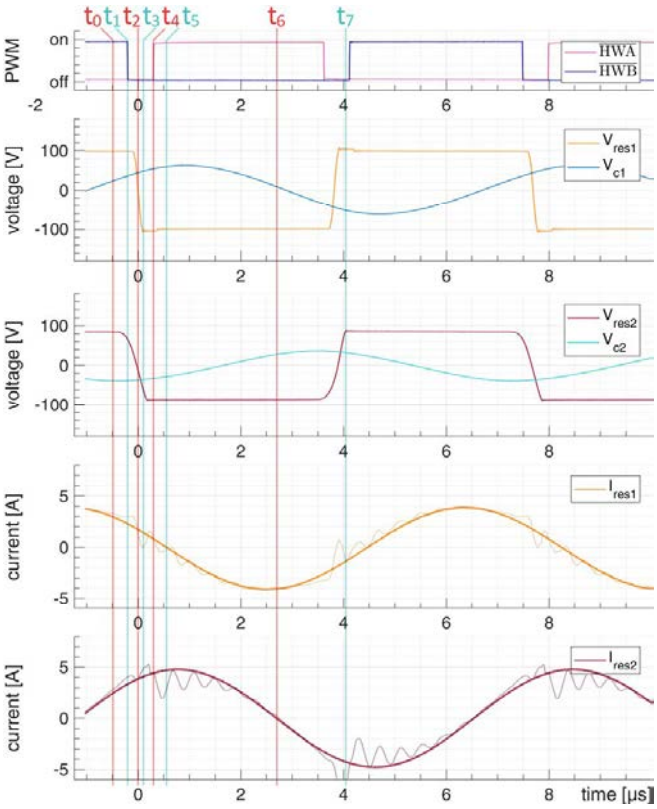

Fig. 7: Q2/3 (HWA) and Q1/4 (HWB) gate signals, resonant tank $V_{res1/2}$ and capacitor $V_{CR1/2}$ voltages, res. currents $I_{res1/2}$ measured on the prototype in forward operation (V_{in} = 100 V, R_{load} = 40 Ω, f_{sw} = 130 kHz). Poor SNR and common mode noise in $I_{res1/2}$ measurements – the thicker lines show their estimated fundamental waves.

2.3 Transfer gain

The ratio of output to input voltage is adjusted by varying the switching frequency f_{sw}. In analogy to the analysis of the LLC converter [19], we use the First Harmonic Approach (FHA) to simplify the circuit diagram in order to calculate its transmission behavior with complex AC theory. In the FHA, only the fundamental waves of the resonant circuit voltages and currents are considered. The input stage is represented by an AC source as seen in Fig. 8 and Eq. (1). The rectifiers and the output load are replaced by an AC load according to Fig. 9 and Eq. (2). Combined with the resonant tank, this results

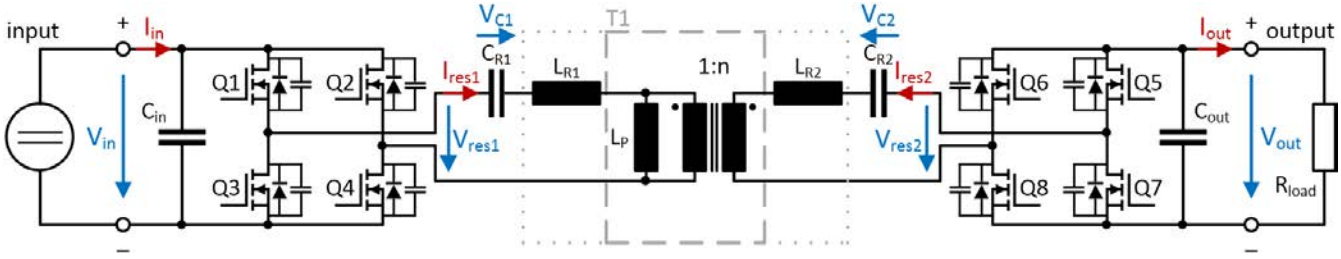

Fig. 6: Simplified topology of a CLLLC converter with full bridges as used in the prototype

in the simplified schematic in Fig. 10, which can be described by Eq. (3) to (5) and the transfer gain M_{G2V} of (6). The gain M_{V2G} in reverse operation mode (i.e. to transfer energy from the EV battery to the grid in V2G mode) is obtained by changing indices 1 and 2 in the formulae and replacing n with 1/n, which returns Eq. (7).

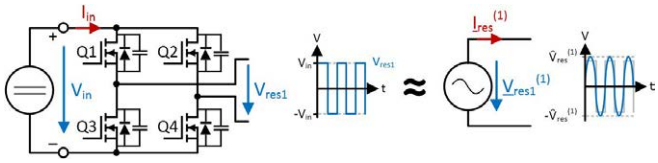

Fig. 8: FHA model of the resonant tank input voltage

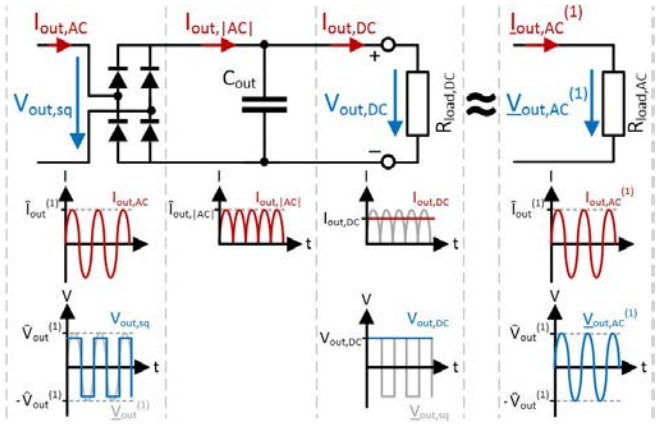

Fig. 9: FHA model of rectifiers and load

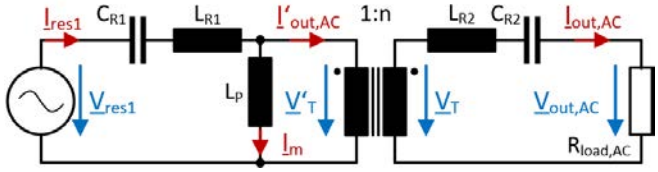

Fig. 10: Final FHA model of the CLLLC converter

$$\hat{V}_{res}^{(1)} = 4/\pi \cdot V_{in} \tag{1}$$

$$R_{load,AC} = \frac{\hat{V}_{out,AC}^{(1)}}{\hat{I}_{out,AC}^{(1)}} = \frac{4/\pi \cdot V_{out,DC}}{\pi/2 \cdot I_{out,DC}} = \frac{8}{\pi^2} \cdot R_{load,DC} \tag{2}$$

$$M := \frac{U_{out,DC}}{U_{in,DC}} \approx \left|\frac{\underline{V}_{out,AC}}{\underline{V}_{res1}}\right| = \left|\frac{\underline{V}_{out,AC}}{\underline{V}_T} \cdot \frac{\underline{V}_T}{\underline{V}_T'} \cdot \frac{\underline{V}_T'}{\underline{V}_{res1}}\right| \tag{3}$$

$$\frac{\underline{V}_T'}{\underline{V}_{res1}} = \frac{j\omega L_P \cdot \underline{I}_m}{j\omega L_P \cdot \underline{I}_m + (j\omega L_{R1} + 1/j\omega C_{R1})\underline{I}_{res1}} \tag{4}$$

$$\frac{\underline{V}_{out,AC}}{\underline{V}_T'} = \frac{R_{load,AC}}{R_{load,AC} + 1/j\omega C_{R2} + j\omega L_{R2}} \cdot n \tag{5}$$

The substitutions illustrated below were used: Primary (f_{res1}) and secondary (f_{res2}) resonance frequency and their relative representation (F_{x1}, F_{x2}), quality factor referred to the primary (Q_1) and secondary (Q_2) side, ratio between primary (m_1) and secondary (m_2) side total to resonant inductance.

$$f_{res1} := \frac{1}{2\pi\sqrt{L_{R1}C_{R1}}} \qquad F_{x1} := \frac{f_{sw}}{f_{res1}}$$

$$f_{res2} := \frac{1}{2\pi\sqrt{L_{R2}C_{R2}}} \qquad F_{x2} := \frac{f_{sw}}{f_{res2}}$$

$$Q_1 := \frac{\sqrt{L_{R1}/C_{R1}}}{R_{load,AC}} \qquad Q_2 := \frac{\sqrt{L_{R2}/C_{R2}}}{R_{load,AC}}$$

$$m_1 := \frac{L_{R1} + L_P}{L_{R1}} \qquad m_2 := \frac{L_{R2} + n^2 \cdot L_P}{L_{R2}}$$

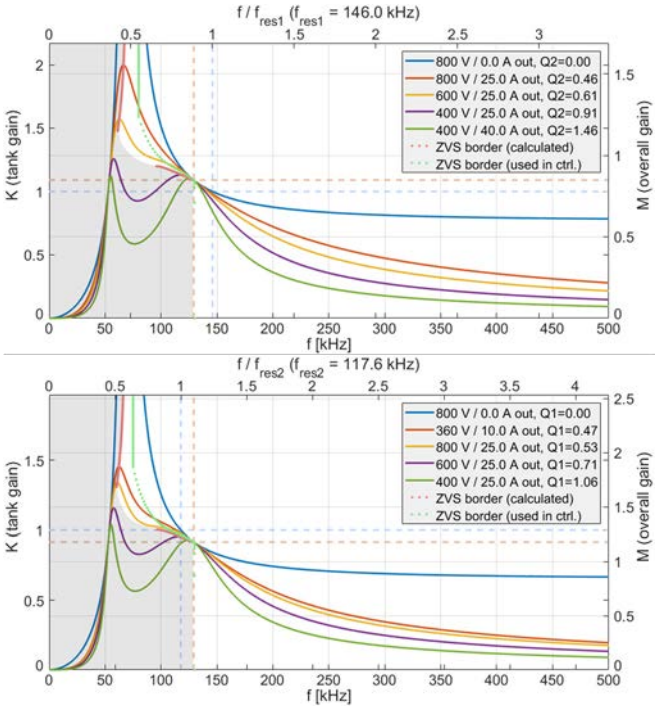

Fig. 11: Transfer gain for G2V (top) and V2G (bottom)

$$M_{G2V} = n \cdot \frac{F_{x1}^2 \cdot (m_1 - 1)}{\sqrt{(F_{x1}^2 m_1 - 1)^2 + (Q_2/F_{x2})^2 \cdot \left(1 - F_{x1}^2 m_1 - F_{x2}^2 m_2 + F_{x1}^2 F_{x2}^2 (m_1 + m_2 - 1)\right)^2}} \tag{6}$$

$$M_{V2G} = \frac{1}{n} \cdot \frac{F_{x2}^2 \cdot (m_2 - 1)}{\sqrt{(F_{x2}^2 m_2 - 1)^2 + \left(Q_1/F_{x1}\right)^2 \cdot \left(1 - F_{x1}^2 m_1 - F_{x2}^2 m_2 + F_{x1}^2 F_{x2}^2 (m_1 + m_2 - 1)\right)^2}} \tag{7}$$

ISBN 978-3-8007-5245-4

The transfer gains of the prototype for varying output loads as a function of the switching frequency f_{sw} in forward/Grid-to-Vehicle (G2V) and backward/Vehicle-to-Grid (V2G) mode are shown in Fig. 11. The overall gain M takes into account both the resonant tank gain K and the transformer winding ratio 1:n. In general, M is lower towards higher f_{sw} and higher load, i.e. the output voltage is lower with a fixed input voltage. The two resonant frequencies f_{res1} and f_{res2} are marked with a blue line. A load-independent frequency f_{li} is marked with a red line. It can be determined by setting the term after $Q_{1/2}$ under the root in Eq. (6) and (7) to 0. f_{li} is independent of the operating direction and equal to f_{res1} and $f_{res\,2}$ if $L_{R1}C_{R1} = L_{R2}C_{R2}$. In the gray region (sometimes reffered to as capacitive area), no ZVS can be achieved on the primary side, because I_{res1} changes its sign (t_5 in Fig. 7) before the turn-on of the next MOSFETs (t_4) and therfore it cannot be used to reverse V_{res1}. In practice, some extra reserve is needed because of the switching dead time. Hence, the controller in the prototype uses the green dotted line as a lower limit for f_{sw}.

2.4 Advantages and drawbacks

As switching losses are almost completely eliminated with ZVS on the input side and ZCS on the output side FETs, the isolated bidirectional CLLLC converter can achieve very high efficiencies and a high power density (partly because less cooling is necessary). This clearly has benefits for use in on-board EV chargers. The resulting electromagnetic radiation may be reduced by soft switching. Due to higher possible switching frequencies, the filters at the input and output as well as the isolating transformer can be reduced in size. However, compared to the LLC or DAB, cost and space requirements for the FETs, the resonant tank capacitors and inductors may increase slightly. With many degrees of freedom, the design process is a bit more complicated than that of a DAB, but a suitable design for the application can yield excellent results in both directions for efficiency and load change behavior. Compared to the DAB, a CLLLC converter can cover larger ranges of output voltage and power with high efficiency and ZVS [9], [12], [14], [17].

3 Simulation

We used different simulation approaches to evaluate the operation of the CLLLC converter before a prototype was set up. The PLECS® Blockset by Plexim was used in Simulink® to simulate the high-level operation of the converter, i.e. (1) to estimate the generated losses, (2) to optimize the controller and (3) to inspect the start-up as well as the fault-behavior of the converter. PLECS® enabled very fast simulations of the converter, because power semiconductors are modeled with ideal switches that are either turned on or off. For this particular reason, soft switching transitions with their finite switching slopes and the effect of parasitic, parallel capacities are difficult to analyze in detail. Therefore, we used LTspice® by Analog Devices to estimate and optimize the switching timings of the MOSFETs and to verify the fundamental operation principle of the resonant tank and its transfer gain.

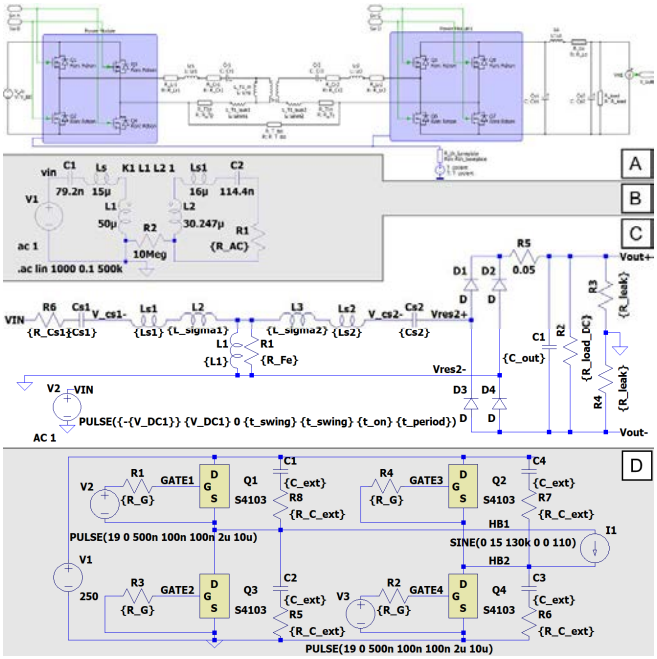

Fig. 12: Segment of the PLECS® (A) and three of the LTspice® simulation models (B, C, D)

Both the results of PLECS® and LTspice® reflect the transfer gain calculated in the FHA model relatively well in most operating points, even if the output voltage was usually a bit lower (see Fig. 13). Slightly larger deviations exist in the capacitive region and at very high switching frequencies.

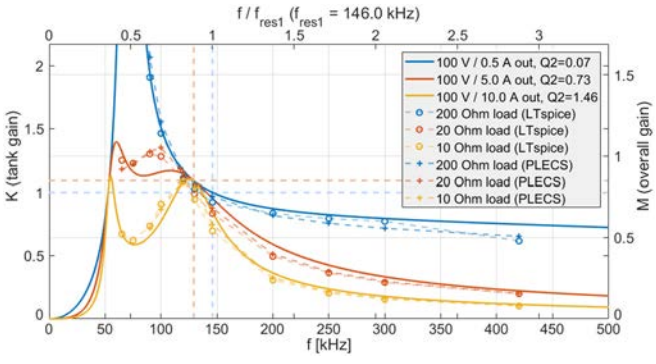

Fig. 13: Calculated (solid lines) and simulated (dashed lines) G2V transfer gains for various loads

ISBN 978-3-8007-5245-4

4 Prototype

4.1 Requirements and application

Based on the results of the theoretical analysis and the simulations, we developed a galvanically isolated, bidirectional DC/DC converter on the basis of a CLLLC resonant circuit (see Fig. 14). The targeted maximum charge/discharge power is 20 kW. The converter is optimized for use in stationary charging points whose primary side is connected to an AC grid with phase-phase voltages of 400 V ± 40 V via a three-phase (3ph) bidirectional AC/DC converter. With conventional voltage-fed two- or three-level inverters, the minimum DC link voltage U_{DC1} at the input of the CLLLC converter is $440\,V \cdot \sqrt{2} \approx 625\,V$. If U_{DC1} is varied between 625 and 800 V depending on the load, the converter is specified to generate output voltages of 200 to 800 V at output powers from 0 kW to up to 20 kW.

With a different design of the resonant circuit, other applications and transfer gains are also conceivable, such as use as a universal on-board charger with AC input voltages ranging from 110 V (1ph) to 400 V (3ph) for a battery voltage of 280 – 400 V.

4.2 Hardware Design

Given the requirements described above, we selected the topology in Fig. 6 was using full bridges at the input and output. Power modules were assembled at our institute (see Fig. 14). They consist of SiC MOSFET bare dies (Cree® CPM3-1200-0013C with a typical $R_{DS(on)}$ of 13 mΩ) without or with additional freewheeling SiC diodes (Cree® CPW5-1200-Z050B or Rohm S6305) or GaAs diodes from 3-5 Power Electronics GmbH.

The resonant circuit components were initially dimensioned to meet the voltage gain requirements. After several simulations, they were iteratively adjusted to reduce the portions of the resonant circuit currents that do not contribute to power transfer, which promised higher efficiency. The final values are shown in . The switching frequency f_{sw} of the converter ranges from 75 to 420 kHz depending on power direction, load and input voltage.

Table 1: Prototype resonant tank component values

L_{R1} [µH]	C_{R1} [nF]	L_{R2} [µH]	C_{R2} [nF]	L_P [µH]	n [ ]	f_{res1} [kHz]	f_{res2} [kHz]
15	79.2	15	114.4	15	7/9	146	117.6

High-speed comparators are used in the resonant tank to detect zero-crossings of $V_{res1/2}$ and whether $I_{res1/2}$ lies above a threshold of ca. 1 A. The signals are used for the synchronous rectification (SR) of the secondary MOSFETs. The signals can help to estimate the duration of the varying primary side FET dead time t_{dead}. They may also be used to detect missing zero-crossings of the primary side V_{res} during the dead time which indicates a lack of ZVS and could prevent hard-switching in advance.

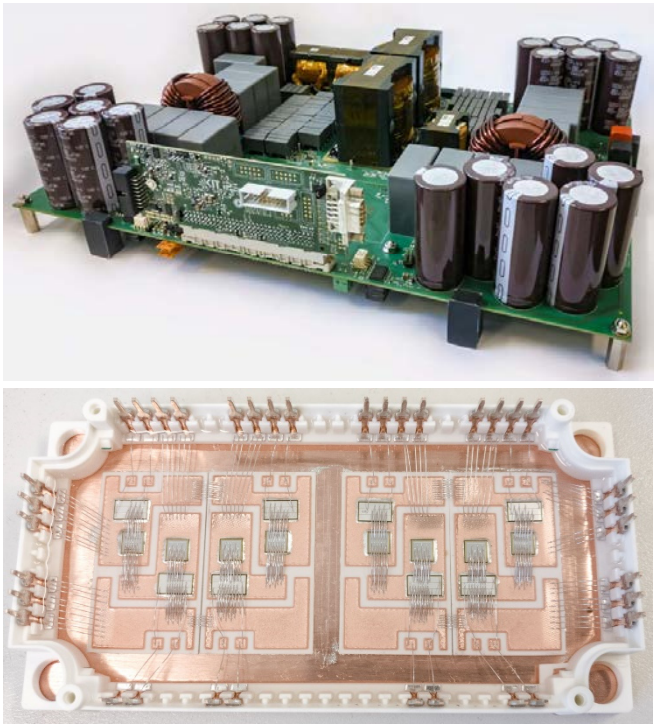

Fig. 14: The 20 kW CLLLC converter prototype and a power module designed and assembled at IPE with two full-bridges (SiC MOSFETs + diodes)

4.3 Software and Controller Design

A fully digital constant current (CC)/constant voltage (CV) battery charging/discharging controller was implemented on an Infineon Aurix™ Tricore™ processor. It is based on an integral controller that starts at a load- and input voltage dependent switching frequency and continuously decreases the switching period T_{sw} until the desired output condition is met. Switching is temporarily stopped in case of an overshoot. Controlling T_{sw} instead of f_{sw} was preferred because of a more linear relationship between the transfer gain M and T_{sw}. The controller fluently shifts between CC and CV modes and may easily be extended with a grid or battery power or maximum device temperature controller.

4.4 Results

4.4.1 Efficiency

The efficiency of the converter is at least 97 % at typical operating points with peaks of more than 98.2 % in both directions (see Fig. 15). However,

ISBN 978-3-8007-5245-4

the efficiency at high output currents still needs to be improved. We achieved significantly higher efficiencies and lower module temperatures using SR on the secondary side and power modules with additional SiC freewheeling diodes with a low forward voltage (see Fig. 16). When SR is enabled, the rectifying MOSFETs turn on whenever the resonant tank voltage and current signals indicate the diodes are conducting a current. However, the turn-on delay of 250 – 350 ns caused largely by the microcontroller has still room for improvement, as this delay represents a noticeable part of the maximum usable on-time (1 - 5 µs) of the rectifying FETs. An FPGA or a dedicated logic gate circuit is likely to improve the efficiency in SR mode even more.

4.4.2 Transfer gain

The measured transfer gain in constant frequency mode matched the FHA gain calculated earlier reasonably well in high load operating points (10-30 Ω curves in Fig. 17). The gain was far higher than expected without load and moderately higher with light loads (40-100 Ω), especially towards higher f_{sw}. Parasitic capacitances of the transformer or the PCB might contribute to this phenomenon, but a clear reason was not yet identified. Despite these phenomena, in practice the CC/CV controller can set the desired operating point without any difficulties by varying f_{sw} or using the light-load burst mode, especially if the occurring gain is higher than calculated in the design stage. As long as the resonant circuit is designed a little conservatively with regard to the desired gain, component variations or temperature dependencies do not pose a problem either. The converter fulfilled typical output voltage or current set point steps after 20-200 ms under load with low overshoot and ripples of less than 2.5 V and 1 A. A light-load mode using switching bursts with variable pauses in between was introduced to operate the converter efficiently at gains lower than presented in Fig. 11 and Fig. 17. Significantly lower output voltages were achieved with little or without load.

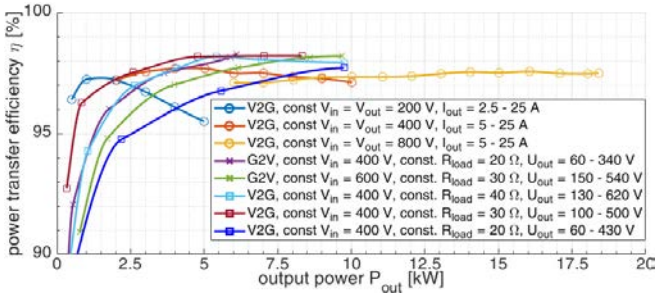

Fig. 15: Power transfer efficiency with freewheeling diodes and SR in different operating conditions (excluding power for cooling and controller)

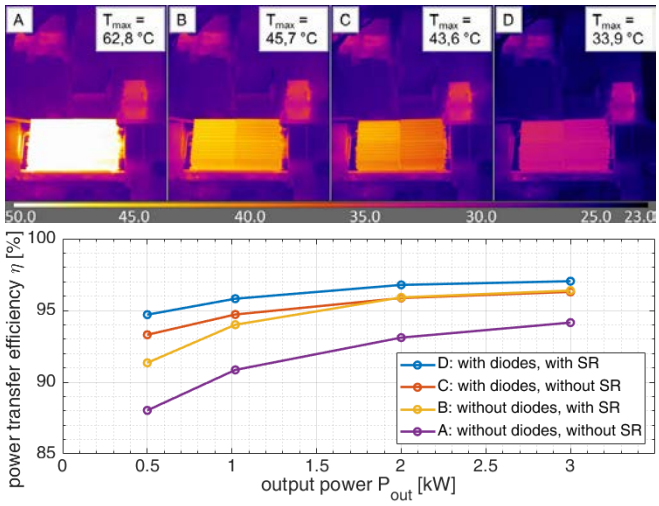

Fig. 16: Thermal images ($P_{out,G2V}$ = 1 kW, T_{amb} = 23°C) and power transmission efficiencies of different air-cooled power modules in steady-state

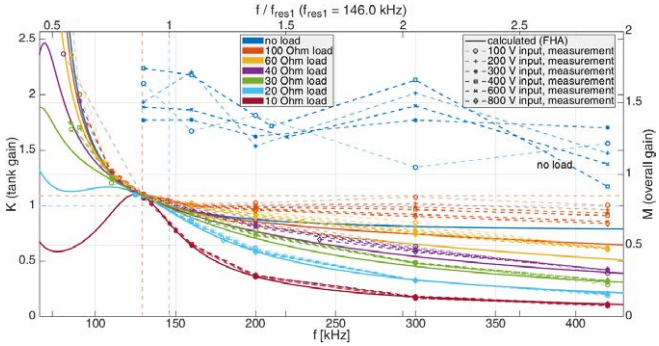

Fig. 17: Transfer gain measured on prototype with various input voltages (markers) and loads (colors)

4.4.3 Switching behavior

With minimum dead times of 200 ns, using fast gate drivers is important. Turn-on times of below 100 ns and turn-off times of less than 150 ns were realized with Rohm BM61M41RFV gate drivers utilizing negative $V_{DS(off)}$ and active Miller clamping for enhanced robustness.

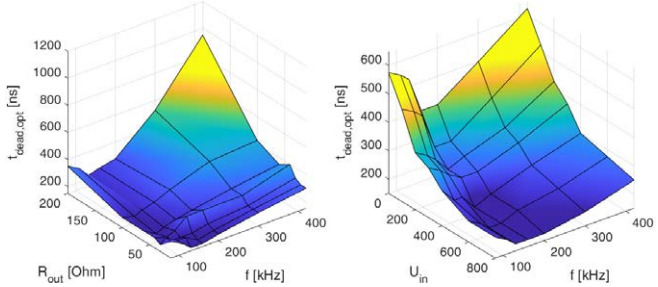

Fig. 18: Minimal t_{dead} to ensure ZVS as a function of f_{sw}, V_{in} and R_{load} with constant V_{in} = 400 V (left) or constant R_{load} = 20 Ω (right) in G2V mode

A variable t_{dead} improved efficiency and ringing since the slope of the input side V_{res} – i.e. the time

needed to reverse the resonant tank voltage for ZVS – differs significantly depending on the input voltage and load (see Fig. 18). A fixed t_{dead} was too short for V_{res} to fully reverse in light load and too long for heavy loads as well as to efficiently use the MOSFET on-time.

5 Conclusion

The bidirectional, galvanically isolated CLLLC converter is a promising DC/DC converter for stationary and on-board chargers to charge EVs and to transfer energy back to the grid for vehicle-to-grid applications. A 20 kW prototype was designed and analyzed based on the calculations and simulations presented in this paper. The prototype was convincing due to a peak efficiency of more than 98.2 %, its compact design and the large voltage gain range that can be achieved with fast response from open circuit to heavy loads.

The performance and efficiency could be improved even more by optimizing the resonant tank to the specific application, for example using an optimization computation to reduce losses and component effort while maintaining the desired voltage gains in all operating conditions.

6 References

[1] M. Schücking, P. Jochem, W. Fichtner, O. Wollersheim, and K. Stella: Influencing factors on specific energy consumption of EV in extensive operations, in 29th International Electric Vehicle Symposium, 2016

[2] W. Kempton and S.E. Letendre: Electric vehicles as a new power source for electric utilities, Transportation Research Part D: Transport and Environment, vol. 2, no. 3, pp. 157–175, 1997

[3] A. Hackbarth, B. Lunz, R. Madlener, D.U. Sauer, and R.W. De Doncker: Plug-in Hybrid Electric Vehicles for CO2-Free Mobility and Active Storage Systems for the Grid (Part 2), 2012

[4] S. Dusmez, A. Cook, and A. Khaligh: Comprehensive analysis of high quality power converters for level 3 off-board chargers, in IEEE Vehicle Power and Propulsion Conference, 2011

[5] I. Batarseh and Ḥarb Aḥmad: Power Electronics : Circuit Analysis and Design, 2. Ed., Springer, 2018

[6] F.C. Lee: High-frequency quasi-resonant converter technologies, Proceedings of the IEEE, vol. 76, no. 4, pp. 377–390, 1988

[7] S.-Y. Yu, R. Chen, and A. Viswanathan: Survey of Resonant Converter Topologies, Texas Instruments Power Supply Design Seminar, 2018

[8] R. Severns: Topologies for three element resonant converters, in Fifth Annual Proceedings on Applied Power Electronics Conference and Exposition, pp. 712–722, 1990

[9] B. Zhao, Q. Song, W. Liu, and Y. Sun: Overview of Dual-Active-Bridge Isolated Bidirectional DC–DC Converter for High-Frequency-Link Power-Conversion System, IEEE Transactions on Power Electronics, vol. 29, no. 8, pp. 4091–4106, 2014

[10] H. Wang and A. Khaligh: Comprehensive topological analyses of isolated resonant converters in PEV battery charging applications, in IEEE Transportation Electrification Conference and Expo, 2013

[11] J. Deng, S. Li, S. Hu, C.C. Mi, and R. Ma: Design Methodology of LLC Resonant Converters for Electric Vehicle Battery Chargers, IEEE Transactions on Vehicular Technology, vol. 63, no. 4, pp. 1581–1592, 2014

[12] S. Zou, J. Lu, A. Mallik, and A. Khaligh: Bi-Directional CLLC Converter With Synchronous Rectification for Plug-In Electric Vehicles, IEEE Transactions on Industry Applications, vol. 54, no. 2, pp. 998–1005, 2018

[13] A. Hillers, D. Christen, and J. Biela: Design of a Highly efficient bidirectional isolated LLC resonant converter, in 15th International Power Electronics and Motion Control Conference, p. DS2b.13-1-DS2b.13-8, 2012

[14] J. Jung, H. Kim, M. Ryu, and J. Baek: Design Methodology of Bidirectional CLLC Resonant Converter for High-Frequency Isolation of DC Distribution Systems, IEEE Transactions on Power Electronics, vol. 28, no. 4, pp. 1741–1755, 2013

[15] W. Chen, P. Rong, and Z. Lu: Snubberless Bidirectional DC–DC Converter With New CLLC Resonant Tank Featuring Minimized Switching Loss, IEEE Transactions on Industrial Electronics, vol. 57, no. 9, pp. 3075–3086, 2010

[16] B. Sen, Chaohui Liu, Jiabin Wang, C. Gould, and K. Colombage: A CLLC Resonant Converter Based Bidirectional EV Charger with Maximum Efficiency Tracking, in 8th IET International Conference on Power Electronics, Machines and Drives, Glasgow, UK, 2016

[17] S. Ditze: Steady-state analysis of the bidirectional CLLLC resonant converter in time domain, in IEEE 36th International Telecommunications Energy Conference, 2014

[18] J. Song, D. Yang, C. Zhang, and B. Duan: Hybrid Control Method for CLLLC Resonant Converter with Low Output Voltage Ripple, IFAC-PapersOnLine, vol. 51, no. 31, pp. 680–684, 2018

[19] S. Abdel-Rahman: Resonant LLC Converter: Operation and Design, Infineon AN 2012-09, 2012